Published in final edited form as:
Nat Struct Mol Biol. 2010 January ; 17(1): 105. doi:10.1038/nsmb.1719.

A Promiscuous α-Helical Motif Anchors Viral Hijackers and Substrate Receptors to the CUL4-DDB1 Ubiquitin Ligase Machinery

Ti Li[1,†], **Eva I. Robert**[3,†], **Pieter C. van Breugel**[3], **Michel Strubin**[3,*], and **Ning Zheng**[1,2,*]

[1] Department of Pharmacology, University of Washington, Seattle, WA 98195 [2] Howard Hughes Medical Institute, Box 357280, University of Washington, Seattle, WA 98195 [3] Department of Microbiology and Molecular Medicine, University Medical Centre, Rue Michel-Servet 1, 1211 Geneva 4, Switzerland

Abstract

The CUL4-DDB1 ubiquitin ligase machinery regulates diverse cellular functions and is frequently subverted by pathogenic viruses. Here we report the crystal structure of DDB1 in complex with a central fragment of hepatitis B virus X protein (HBx), whose DDB1-binding activity is essential for viral infection. The structure reveals that HBx binds DDB1 through an α-helical motif, which is also found in the unrelated paramyxovirus SV5-V protein despite their sequence divergence. Our structure-based functional analysis shows that, like SV5-V, HBx captures DDB1 to exploit the ubiquitin ligase activity of the CUL4-DDB1 E3. Based on the shared action mechanisms of the two viral proteins, we further identify the same α-helical motif in the substrate-recruiting subunits of the cellular E3 complex, DCAFs, which are functionally mimicked by the viral hijackers. Together, our studies reveal a common yet promiscuous structural element important for the assembly of viral and cellular substrate receptors into the core complex of the CUL4-DDB1 ubiquitin ligase.

INTRODUCTION

Protein ubiquitination is a widespread post-translational modification that regulates the activities of myriad eukaryotic proteins in diverse cellular functions[1]. In order to conjugate ubiquitin to various protein targets with high specificity, eukaryotic cells have evolved a large number of enzymes, known as ubiquitin E3 ligases, that can each recognize one or a limited set of specific protein substrates and catalyze the ubiquitin transfer reaction together with ubiquitin-activating E1 and ubiquitin-conjugating E2 enzymes[2]. The cullin-RING ligases represent the largest super-family of multi-subunit E3 ubiquitin ligase complexes in eukaryotic cells[3]. Organized by a catalytic core consisting of a cullin scaffold and the RING domain protein Rbx1/Roc1, the cullin-RING complexes all feature interchangeable substrate receptor subunits, which are docked to the E3 ligase platform through an adaptor. By combining different substrate receptors with the same catalytic core, the cullin-RING E3 complexes greatly expand their substrate repertoire while maintaining high specificity. In humans, six closely related cullin proteins (CUL1, CUL2, CUL3, CUL4A, CUL4B, and CUL5) have been identified, each capable of assembling a distinct family of E3 complexes. Using Skp1 and

*Correspondence: nzheng@u.washington.edu; michel.strubin@unige.ch.
†These authors contributed equally to this work.

The Protein Data Bank accession numbers for the DDB1-HBx, DDB1-WHx, DDB1-DCAF9, and DDB1-DDB2 structures are WWWW, XXXX, YYYY, and ZZZZ.

Skp1-like adaptors, CUL1–3 and CUL5 share a common structural mechanism to nucleate different cullin-RING E3 complexes.

Recent studies have shown that the human CUL4A and CUL4B proteins can both interact with the evolutionally conserved DDB1 adaptor protein and assemble a unique family of cullin-RING ligase complexes, hereafter referred to as the CUL4-DDB1 E3s[4–7]. Cellular functions regulated by CUL4-DDB1 E3s include, but are not limited to, DNA repair[8–14], DNA replication[5,14–18], transcription[19], and signal transduction[20,21]. Distinct from all other cullin adaptors with the Skp1/BTB fold, DDB1 is a large multi-domain protein consisting of three β-propeller domains (BPA to BPC) and a C-terminal α-helical fold[22]. In DDB1, the BPB domain interacts with the N-terminal end of the CUL4 scaffold, whereas the structurally coupled BPA-BPC double-propeller fold is responsible for docking a family of substrate receptor proteins, known as DCAFs (DDB1-CUL4-Associated Factors)[4,5] or DWDs (DDB1-binding WD40 proteins)[6]. Although the cellular functions of many DCAFs remain poorly understood, most of them are characterized by a WD-repeat domain in their primary sequences. Analogous to the ones found in some of the SCF substrate receptor F-box proteins, such as β-TrCP and Fbw7[23,24], the WD-repeat domains of DCAFs potentially provide the substrate-binding sites on the CUL4-DDB1 E3 complexes. Lacking a conserved DDB1-binding motif outside the WD-repeat domain, however, how DCAFs are selectively recognized by DDB1 among all WD-repeat proteins remains unclear. A double DxR motif on the surface of the WD-repeat domains of DCAFs and a DWD motif within the DCAF WD-repeat sequences have been separately proposed as the signature motif for the CUL4-DDB1 substrate receptors[4–6]. Yet, neither motif is strictly shared among all experimentally identified DCAFs, suggesting that a more complex mechanism might underlie the specific docking of DCAFs to DDB1.

As widely expressed cellular ubiquitin ligases, the cullin-RING E3 complexes are frequently subverted by pathogenic viruses[3]. By bridging a cellular target to the adaptor or a substrate receptor of a cullin-RING E3, a number of viral proteins are able to hijack the cellular E3 machinery for ubiquitinating and degrading anti-viral or regulatory factors of the host. One of the best examples is the exploitation of the CUL4-DDB1 E3 by the paramyxovirus V protein, which can functionally mimic DCAFs to directly dock to DDB1 and simultaneously interact with one of the STAT proteins in the interferon signaling pathway[25–27]. Upon recruiting a STAT protein to the CUL4-DDB1 ligase complex, the V protein promotes the polyubiquitination and rapid turnover of the key signal tranducer, thereby, blocking the anti-viral response of the host cells. The hepatitis B virus X protein (HBx), which plays an essential role in viral replication in vivo[28], is a second viral protein known to specifically interact with DDB1[29]. Although the precise mechanism by which HBx mediates viral replication remains elusive, its normal interaction with DDB1 is essential for efficient viral infection as well as its reported activities in cultured cells, including stimulation of viral genome replication and induction of genetic instability and subsequent cell death[30–34]. In this study, we show that, despite sequence diversity, HBx anchors itself on DDB1 through an α-helical motif that is also used by the paramyxovirus V protein. Similar to the paramyxovirus V protein, HBx requires the intact CUL4-DDB1 complex, thereby, the ligase function of the E3 machinery, to retain its activities. Upon revealing the common structural element used by both viral proteins to functionally mimic DCAFs, we further identify a similar and previously unrecognized α-helical motif in the cellular substrate receptors of the CUL4-DDB1 ubiquitin ligase critical for the assembly of the modular E3 machinery.

RESULTS

Crystal structures of DDB1 in complexes with hepatitis virus X protein peptides

The hepatitis B virus X protein (HBx) is a 17 kDa small regulatory protein conserved among mammalian hepadnaviruses[29]. Like HBx, the woodchuck hepatitis virus X protein (WHx) also

shows the DDB1-binding activity, which is essential for efficient viral infection *in vivo*[35,36]. Previous studies have mapped a partially conserved short sequence motif in HBx and WHx important for DDB1 association[37] (Fig. 1a). To unravel the structural basis of the interaction between DDB1 and the viral X proteins, we have determined the crystal structures of human DDB1 in complexes with peptides corresponding to these central fragments of HBx and WHx (Table 1). The DDB1-HBx complex structure reveals that the HBx peptide adopts a 3-turn α-helical conformation and binds to DDB1 at the large pocket enclosed by its BPA-BPC double propeller fold (Fig. 1b). With few contact to the DDB1 BPA domain, the HBx peptide predominantly interacts with the "top" surface of the DDB1 BPC domain. Most, if not all, DDB1-interacting residues of the viral peptide are located at the bottom side and the two ends of the α-helical structure. At the opening of the DDB1 double propeller pocket, the N-terminal end of the HBx peptide helix interacts with a DDB1 loop (4b–4c loop) projecting from the BPC domain. Deep inside the pocket, the viral sequence ends its helical conformation and points its very C-terminus back toward the entrance of the DDB1 pocket (Fig. 1b).

The WHx peptide adopts the same helical conformation as HBx does upon interacting with DDB1, albeit their rather divergent sequences (Fig. 1c,d,e). The two viral DDB1-binding sequences have only three invariant amino acids, all of which are found at the C-terminal end of the helical motif (Fig. 1a). Of these three conserved residues, the viral Arg residue (Arg96 of HBx and Arg94 of WHx) forms two hydrogen bonds with DDB1; the viral Leu residue (Leu98 of HBx and Leu96 of WHx) is accommodated by a hydrophobic patch on the DDB1 BPC domain formed among Leu328, Pro358, and Ala381, Phe382; and the viral Gly residue (Gly99 of HBx and Gly97 of WHx) terminates the helix (Fig. 1c). In both structures, this part of the interface is further strengthened by two DDB1 residues, Arg327 and Asn1005, each donating a hydrogen bond to a carbonyl group of the helical peptide backbone (Fig. 1c).

The sequences of the N-terminal halves of the HBx and WHx helical motifs are noticeably divergent, with no strictly conserved amino acid (Fig. 1a). Most DDB1-contacting residues in this part of the two X proteins, nevertheless, show overall conserved side chain properties and contribute to the DDB1 interaction in a conserved fashion. In particular, Phe87, Val88, and His91 of WHx and their corresponding HBx residues mediate the intermolecular docking by packing against several fixed residues on the "top" surface of the DDB1 BPC domain (Fig. 1d). Superposition analysis of the two structures, on the other hand, reveals unexpected structural differences in DDB1 upon interacting with the two different X proteins. In the DDB1-WHx complex, three hydrogen bonds are formed between the N-terminal end of the viral helix and the DDB1 4b-4c loop, two made by the first amino acid of the viral helical motif (Asn96), whereas in the DDB1-HBx structure, the DDB1 loops is pushed further out by the viral helix, making only hydrophobic and van der Waal contacts with the N-terminal end of viral peptide (Fig. 1d). Next to the middle part of the viral helices, another surface loop of the DDB1 BPC domain also adopts different conformation in the two complex structures (Supplementary Fig. S1). Thus, the combination of the hydrophobic surface properties and the intrinsic plasticity of the "top" surface of the DDB1 BPC domain allow it to accommodate the viral helical motifs with significant sequence variation. Overall, the two viral peptides fold into a similar short α-helix and anchor themselves deeply into the large DDB1 double propeller pocket, burying a total of ~800 $Å^2$ surface area.

Structure comparison of the DDB1-binding motifs of HBx and SV5-V

The helical DDB1-binding motif of the viral X proteins is reminiscent of the paramyxovirus SV5-V protein, which also contains an N-terminal helical sequence interacting with the DDB1 double propeller pocket[22]. Superposition analysis shows that the SV5-V N-terminal sequence and the two X protein peptides adopt essentially the same helical structure and occupy the same surface area on the DDB1 BPC domain (Fig. 1e). Strikingly, the amino acid sequence of the

SV5-V helical motif is significantly different from the HBx helical motif (Fig. 1a). Consistent with the lack of detectable sequence homology between the unrelated viral V and X proteins, the DDB1-binding motifs of HBx, WHx, and SV5-V have no single amino acid in common when they are aligned based on the structures (Fig. 1a). None of the three invariant residues between HBx and WHx at the C-terminal part of the helical motif is conserved in SV5-V. Only when aligned in pairs does the helical motif of WHx show sequence similarity to each of the other two, but in non-overlapping positions (Fig. 1a).

Close examination of the interfaces in all three structures reveals several common key contacts made by the viral motifs through amino acids of the same or similar types. For instance, all the hydrophobic residues of the SV5-V helix (Val24, Phe27, and Val32) form hydrophobic interactions with the same DDB1 residues as their corresponding residues in HBx and WHx do. The same hydrogen bond network formed among the backbone groups of the WHx peptide and the surface residues of the DDB1 BPC domain is also found in the DDB1-SV5-V structure. Together, these analyses indicate that the completely unrelated paramyxovirus V and hepatitis virus X proteins share a common mechanism for DDB1 interaction, which involves the docking of a short α-helical viral motif formed by relatively variable sequences to DDB1.

The BPA-BPC double propeller of DDB1 as the major HBx-binding site

To verify the crystallographic results in the context of the full-length proteins, we performed a series of structure-based mutation analyses of DDB1. We first investigated whether the binding of full-length HBx involves the structurally independent BPB domain of DDB1, which is closely connected to the BPC domain (Fig. 1b). Wild-type DDB1 and a deletion mutant lacking the entire BPB domain were fused in frame to the VP16 activation domain and tested in a yeast two-hybrid assay for interaction with HBx, WHx, and SV5-V linked to the DNA-binding protein RFX. Figure 2a shows that the VP16-DDB1 truncation mutant lacking the BPB domain activates an RFX-dependent *lacZ* reporter gene comparably to the wild type DDB1 protein when expressed in combination with RFX-HBx or RFX-WHx. The same is true when SV5-V is used as bait (Supplementary Fig. S2). These results suggest that HBx and WHx interact with only the BPA-BPC module of DDB1, as SV5-V does in the crystal structure of the DDB1-SV5-V complex[22].

We next probed the importance of the "top" surface of the DDB1 BPC domain for holding the full-length viral X proteins in place. Our analysis focused on two DDB1 amino acids, Ala381 and Phe382, which pack against the HBx Leu98 residue deep inside the DDB1 double propeller pocket (Fig. 1c). As shown in Figure 2b, a DDB1 double mutant bearing charged substitutions at these two positions (A381E/F382D) effectively disrupts the binding of DDB1 to both full-length HBx and WHx, and also impairs DDB1 association with SV5-V (Fig. 2b and Supplementary Fig. S2). The DDB1 double mutant exhibits normal binding to a cellular DDB1 partner of unknown function[4], Trpc4AP, which also interacts with the DDB1 double propeller (Fig. 2b and Supplementary Fig. S2). This control experiment indicates that mutations of the two DDB1 residues abolish viral protein binding without affecting the proper folding of DDB1. Consistent with these results, mutation of Leu98 within HBx has been shown to compromise its binding to DDB1[33]. Taken together, the above mutational analyses underline the importance of the interface between the viral helical motif and the "top" surface of the DDB1 BPC domain for intact HBx-DDB1 complex formation.

The viral helix-DDB1 interface is critical for HBx-induced cytotoxicity

To test the functional importance of the interaction between DDB1 and the viral X protein helical motif, we next examined whether HBx would retain deleterious activities in mammalian cells expressing the DDB1 mutant defective for HBx binding in place of endogenous DDB1. Because DDB1 is essential for viability of proliferating cells[38,39], we first established that the

DDB1(A381E/F382D) double mutant can functionally substitute for the wide type DDB1 for cell viability and proliferation. Figure 2c shows that silencing of DDB1 by transfection of an episomal vector directing the synthesis of a DDB1-specific small interfering RNA (siRNA) inhibits HeLa cell growth in a colony formation assay, as expected (Fig. 2c, upper panel). These cells can be largely rescued by transfection with an siRNA-resistant form (SiR) of wild-type DDB1 and, to a slightly lesser extent, with the DDB1(A381E/F382D) double mutant, but not by transfection with wild-type DDB1 (Fig. 2C, lower panel). Western blot analysis using HA-epitope tagged DDB1 to distinguish from the endogenous protein demonstrates that the siRNA-mediated knockdown of DDB1 is efficient and specific and that the $DDB1^{SiR}$ variants are expressed at close to normal levels (Supplementary Fig. S3).

To assess for HBx cytotoxic activity in the DDB1(A381E/F382D) mutant background, we generated HeLa cells depleted for DDB1 by siRNA and expressing the siRNA-resistant version of either wild-type DDB1 or the DDB1(A381E/F382D) double mutant. The transfected cells were then transduced with lentiviral vectors encoding GFP, GFP-HBx or the GFP-HBx(R96E) point mutant, which is defective for DDB1 binding as we have reported before[33]. Figure 2d demonstrates that transduction efficiency as determined 5 days later by FACS analysis for GFP fluorescence was high in all cases (Fig. 2d, left panel). A very similar FACS profile was obtained at 16 days after transduction with cells transduced with GFP or the GFP-HBx(R96E) mutant (Fig. 2d, right panel), indicating that expression of these proteins confers no major growth disadvantage to cells. By contrast, the proportion of GFP-HBx-expressing cells markedly decreased in control cells normally expressing endogenous DDB1 and in cells complemented with the wild-type $DDB1^{SiR}$ variant (Fig. 2d, right panel), consistent with HBx exerting deleterious activities in these cells. This, however, did not occur when cells were complemented with the HBx-defective $DDB1(A381E/F382D)^{SiR}$ mutant. In fact, most cells in this case remained GFP-positive at day 16 (Fig. 2d, right panel) and showed proliferation in a colony formation assay (Supplementary Fig. S4). Thus, HBx is expressed yet largely lacks cytotoxic activities in these cells. This result unequivocally demonstrates that HBx acts through its interaction with DDB1 and binding of the viral helical motif to the “top” surface of the DDB1 BPC domain is essential for HBx activities.

HBx binds DDB1 to reprogram the CUL4 E3 ubiquitin ligase

The common DDB1-binding motif shared between the hepatitis X protein and the paramyxovirus V protein suggests that HBx may function as SV5-V does by subverting the normal function of the cellular ubiquitin ligase complex. Alternatively, HBx could inhibit the activities of the CUL4-DDB1 E3 machinery to fulfill its role. To distinguish these two possibilities, we first probe whether HBx can physically integrate into the CUL4A-DDB1 complex. Figure 3a (lower panel) shows that upon co-transfection both HA-DDB1 and Myc-Cul4A can be coimmunoprecipitated efficiently with GFP-HBx but not with a GFP control from extracts of HeLa cells. Much lower amounts of myc-Cul4A and HA-DDB1 are recovered when the experiment is performed with the HBx(R96E) mutant defective for DDB1-binding.

Next, we generated a CUL4-binding defective mutant of DDB1 to test whether CUL4 and the rest of the E3 ubiquitin ligase complex are in fact required for HBx activities. Our previous structural studies revealed that CUL4A interacts with DDB1 by contacting both the “top” surface and one peripheral side of the DDB1 BPB domain[22]. Although simultaneous mutations of three critical residues (W561K, I587D and R589E) on the “top” surface of the DDB1 BPB domain was not sufficient to disrupt the binding of DDB1 to CUL4A (data not shown), introduction of a fourth amino acid substitution, A400D, at the peripheral side of the DDB1 BPB domain completely abolished complex formation as assessed by coimmunoprecipitation analysis (Fig. 3b). Because the resulting mutant, DDB1(m4), fails to substitute for endogenous DDB1 (data not shown), we tested the mutant for its ability to support HBx-induced

cytotoxicity following a previously established method. Our previous studies have shown that a covalent link between HBx and DDB1, by acting as a "clamp" forcing the two protein together, can restore the activities of the HBx(R96E) DDB1-binding mutant[40]. Figure 3c shows that, with the same expression level, HBx inhibits cell growth in a colony-forming assay when fused to wild-type DDB1, as expected, but not when fused to the DDB1(m4) mutant. Hence, HBx cytotoxic activity requires DDB1 binding to CUL4A and, likely, the ubiquitin ligase activity of the cellular E3 complex.

To determine whether HBx has similar requirements for stimulation of HBV replication, we made use of an HBx-dependent replication system in which the HBx function can be provided in *trans*[31]. In this assay, human hepatoma cells are transfected with either a wild-type HBV genomic construct or a mutant lacking a functional HBx gene, with or without cotransfection of an HBx expression plasmid. The amount of viral DNA replicative intermediates recovered from purified cytoplasmic core particles is quantified by real time PCR. As seen in Figure 3c, replication of the HBx-deficient HBV genome is strongly reduced compared to the wild type. It is restored by cotransfection of HBx but not the HBx(R96E) DDB1-binding mutant. Remarkably, both wild-type HBx and the HBx(R96E) mutant exhibit stimulatory activities when fused to native DDB1. Yet, they are essentially inactive when linked to the CUL4A-binding defective DDB1(m4) mutant. The same was observed when the HBx fusions were tested for their ability to stimulate transcription of a luciferase reporter gene placed under control of the HBV enhancer I and associated promoter element (Supplementary Fig. S5). These results highlight the importance of DDB1 binding to CUL4A for HBx activities and implicate that HBx interacts with DDB1 to exploit the ligase function of the cellular E3 machinery instead of inhibiting it. The precise substrate ubiquitinated by the HBx-hijacked CUL4-DDB1 E3 complex awaits future investigation.

DCAF9 contains an α-helical motif critical for DDB1 binding

By reprogramming the cellular CUL4-DDB1 E3, the viral X and V proteins functionally mimic DCAFs, the modular substrate receptors of the E3 complex. The common DDB1-docking mode adopted by the two viral proteins raises the possibility that docking of DCAFs to DDB1 might involve the same helical motif, a structural mechanism also mimicked by the viral proteins. Our previous studies have shown that the WD-repeat-containing DCAF proteins interact with DDB1 on its BPA-BPC double propeller fold[4]. If DCAFs indeed bind to the "top" surface of the DDB1 BPC domain, the X protein peptides should be able to compete with DCAFs for DDB1 binding. We tested this in an *in vitro* pull-down assay with purified recombinant proteins. As seen in Figure 4a, DDB1 shows robust interaction with GST-fused DCAF9, a DCAF protein identified in our previous proteomic studies and also known as WDTC1[4], whereas the two proteins can no longer form a stable complex when DDB1 is preloaded with the α-helical DDB1-binding peptide of WHx. This result suggests that either the "top" surface of the DDB1 BPC domain is directly involved in DDB1-DCAF9 interactions, or the subtle conformational changes induced by the viral peptide binding might indirectly perturb the DDB1-DCAF9 interface.

The WD-repeat domains of most DCAFs are formed exclusively by β-strands, which fold into a globular β-propeller fold. It is, therefore, unlikely that the DCAFs use their WD-repeat domain to interact with the "top" surface of the DDB1 BPC domain as the viral helical sequences do. As DCAF9 has sequence extensions beyond both ends of its predicted WD-repeat domain, we hypothesized that these regions outside the WD repeats might be responsible for contacting the DDB1-BPC "top" surface. Indeed, binding analysis with a series of DCAF9 truncation mutants shows that removal of the N-terminal 26 amino acids is sufficient to abolish DCAF9-DDB1 interaction, whereas C-terminal truncation of DCAF9 has little effect (Fig. 4b,c). Intriguingly, amino acids 5 to 17 in the N-terminal sequence of DCAF9 is predicted to

be an α-helix and shows moderate sequence similarity to the WHx DDB1-binding helix (Fig. 5b). These properties of the DCAF9 N-terminal sequence strongly suggest that the DCAF9 substrate receptor of the CUL4-DDB1 E3 might also use a short α-helical motif to dock to the DDB1 at the double propeller pocket.

In order to validate this possible structural role played by the DCAF9 N-terminal sequence, we determined the crystal structure of DDB1 in complex with a peptide corresponding to amino acids 5 to 17 of the DCAF protein (Table 1). Consistent to our binding analysis and the secondary structure prediction result, the DCAF9 peptide adopts a helical conformation and interacts with the "top" surface of the DDB1 BPC domain in exactly the same manner as the three viral proteins do (Fig. 5a,c). Despite considerable sequence variation in the N-terminal half, the short helical DDB1-binding motif of DCAF9 makes similar contacts with DDB1 as observed in the viral protein-DDB1 complexes. This result, once again, underscores the capability of the DDB1 BPC domain to accommodate variable helical sequences through its "top" surface. Importantly, it definitely shows that a DCAF protein binds DDB1 through an α-helical motif anchored at the DDB1 double propeller pocket and such a binding mode is mimicked by the viral hijackers. Given the α-helical structure of the motif and its presence in the HBx protein, we name it the H-box.

H-box in substrate receptors of the CUL4-DDB1 E3

In the primary sequence of DCAF9, the H-box motif is located about 30 amino acids N- terminal to the first predicted β-strand of the WD-repeat domain. To reveal whether other DCAF proteins also have such a short motif, we scrutinized the sequences of other DCAFs in the similar region and searched for a short sequence that is predicted to adopt an α-helical secondary structure and shares a similar sequence pattern with the H-box motifs from DCAF9 and the three viral proteins. Based on the four available crystal structures, we outlined the H-box motif as a 13 amino acids sequence with a non-charged polar residue or a non-aromatic hydrophobic residue at position 1, generally hydrophobic residues at position 2, 3, and 6, and a Val/Leu/Ile residue at position 11. Furthermore, an Arg residue is preferentially found at position 9 and a Gly residue is preferentially located at either position 12 or 13. In six additional DCAFs (DDB2, DCAF4, DCAF5, DCAF6, DCAF8, and DCAF12), a potential H-box motif can be identified fitting the criteria above (Fig. 5b). Due to their sequence divergence and short length, these motifs were not recognized in previous analysis, although a truncation mutant of DDB2 lacking part of the predicted H-box motif has been previously shown to be important for DDB1-DDB2 interaction[5]. To verify that these predicted helical motifs in DCAFs indeed interact with DDB1 like the H-boxes in DCAF9 and the viral proteins, we determined the crystal structure of DDB1 in complex with a peptide corresponding to the predicted motif in DDB2. Previous studies have shown that an eleven amino acid region of DDB2 overlapping the predicted H-box motif is important for DDB2-DDB1 association[5]. As shown in Figure 5c, the DDB2 peptide is indeed α-helical and binds DDB1 in the same fashion as the ones from DCAF9, HBx, WHx, and SV5-V. We therefore conclude that at least a major fraction of the substrate receptors of the CUL4-DDB1 ubiquitin ligase uses the H-box motif to bind the DDB1 adaptor protein, a structural mechanism that is also employed by viral hijackers of the cellular E3 complex.

DISCUSSION

While our current studies have identified the H-box motif as a critical structural element used by both viral and cellular substrate receptors to bind DDB1, several lines of evidence suggest that it is not the only structural contact made by these substrate receptor proteins to dock to the CUL4 adaptor protein. In the crystal structure of the DDB1-SV5-V complex, the paramyxovirus V protein features a C-terminal globular zinc-binding domain that closely interacts with the DDB1 BPC domain outside its "top" surface[22]. Previous deletion analysis

indicated that both the H-box motif and the zinc-binding domain of SV5-V are important for DDB1 binding[41]. Our studies suggest that such a bipartite binding mechanism might be also true for HBx, whose residues outside the H-box sequence also contribute to DDB1 association[33]. Similar to the viral hijackers, DCAFs might interact with DDB1 via multiple interfaces, which involve not only the H-box motif but also other parts of the polypeptides, most likely the common WD-repeat domain. In fact, our previously proposed tandem double DxR motif on the "bottom" surface of the WD-repeat domains of DCAFs might mediate such interactions, as point mutations in the double DxR motif in several DCAFs effectively abrogate DDB1 binding[4]. As shown in Figure 6, we propose that HBx and most WD-repeat domain-containing DCAF proteins interact with DDB1 through a bipartite interface. Inside the DDB1 double propeller pocket, the short and helical H-box motif of HBx and DCAFs docks to the "top" surface of the DDB1 BPC domain. Outside the DDB1 pocket, another domain of HBx and the WD-repeat domain of DCAFs might reinforce the assembly by anchoring to the DDB1 double propeller outside the pocket. Although we have found the H-box motif in a total of seven DCAF proteins with high confidence, it is very likely that such a motif also exists in other DCAFs and possibly involves even more divergent sequences. While the functional advantage for DCAFs to have such a bipartite interface with DDB1 remains to be understood, it might provide a unique mechanism for the CUL4-DDB1^{DCAF} E3 complex to switch between productive and non-productive forms of a E3 machinery without completely disassembling the ubiquitin ligase complex.

METHODS

Protein expression and purification

Full-length human DDB1 was expressed and purified as described previously[22]. GST tagged full-length DCAF9/WDTC1 and its truncation mutants were expressed in *E. coli* and isolated from soluble cell lysate by glutathione affinity chromatography.

Structure determination and refinement

DDB1 was crystallized under the same condition as before[22]. Single DDB1 crystals were soaked with 1mM peptide in crystallization reservoir solution for three hours and subsequently frozen in a cryoprotectant solution in liquid nitrogen for data collection. The DDB1-peptide crystals have the same space group, unit cell, and number of molecules in an asymmetric unit as the crystals of DDB1 alone. With the published DDB1 structure as search model, structures of the DDB1-HBx, DDB1-WHx, DDB1-DCAF9, and DDB1-DDB2 complexes were determined by molecular replacement using the program Phaser[42]. The peptide models were built in with COOT or O [42,43]. CNS and Refmac were used for model refinement[44]. The final parameters of the each structure are laid out comparatively in Table I.

GST pull-down assays

GST tagged full-length DCAF9 and its truncation mutants were left on the glutathione sepharose beads after affinity purification from *E. coli* cultures. DDB1 was mixed with excessive amount of peptide WHx before passed through the beads. After extensive wash, proteins left were eluted from the beads and analyzed by SDS-PAGE with Coomassie staining.

Mammalian Expression Constructs

GFP, GFP-HBx and GFP-HBx(R96E) expressed from the lentiviral vector pWPTS (Fig. 2d and S4) and from the episomal vector EBS-PL (Fig. 5a) have been described[31]. DDB1, the HA-tagged DDB1 version carrying a triple HA epitope at the N terminus[32], and mutants thereof were produced from EBS-PL except in Figure 5b where the HA-DDB1 proteins were made from pSRαS. The DDB1-specific small interfering RNA (siRNA) was produced from the pLV-

TH lentiviral vector carrying a GFP marker[31] in Figure S4 and from EBB-SUP[40] in all the other Figures. The myc-epitope tagged CUL4A in pcDNA has been described previously[22]. The HBx-DDB1 and HBx(R96E)-DDB1 fusions, all variants thereof, and the control HBx and HBx(R96E) point mutant were all expressed from EBS-PL. The replication-competent wild-type HBV genomic construct (payw1.2) and the HBx-deficient derivative (payw*7) used in Figure 5d has been previously published[31]. The luciferase reporter construct used in Figure S5 is driven by a 550-bp restriction fragment derived from payw1.2 and containing the HBV Enhancer I and associated X gene core promoter. The fragment was cloned upstream of the luciferase coding region into pGL3 (Promega) using a naturally occurring *Nco*I site overlapping the ATG initiator codon of the X gene. DDB1(ΔBPB) was generated by ligation of two PCR products to replace the entire BPB domain (from I396 to Q708) by 2 glycine residues linking BPA to BPC. DDB1(A381E, F382D) and the CUL4-binding defective DDB1(m4) mutants were produced by multistep PCR mutagenesis using partially overlapping primers. The siRNA-resistant (SiR) DDB1 versions used in Figure 2 contain three silent mutations in the region covered by the siRNA. All constructs were verified by partial sequencing. Details of the plasmid constructions are available upon request.

Cell Culture, Transfection and Transduction

HeLa cells and the human hepatoma HepG2 cell line were grown exactly as described[34]. Cells seeded the day before at a density of ~10^5 total cells per 30-mm-diameter well (~8×10^5 HepG2 cells in the replication assay[31]) were transfected using FuGENE 6 (Roche), or JetPEI (PolyPlus Transfection) in Figures 5a and 5b, following the manufacturer's instructions. When needed, a GFP expression plasmid was cotransfected (10% of total DNA) to assess transfection efficiencies. Total DNA amount was kept equal using empty vectors. Transfection efficiencies estimated 24-h later by fluorescence-activated cell sorting (FACS) analysis were generally 50–70% with HeLa cells and around 5% with HepG2 cells. Lentiviral transduction was with an MOI of 5 as described before[31].

Immunoprecipitation and Western Blot Analysis

The coimmunoprecipitation experiments in Figures 5a and 5b were performed with whole-cell extracts prepared 24-h post-transfection from 2×10^5 HeLa cells collected with Versene (Invitrogen) as described[34], except that glycerol was added at 17% final concentration after cell lysis. Western blot analyses were performed by transfer of proteins to PVDF Hybond-P membranes (Amersham). The membranes were probed with 1:1,000 rabbit anti-GFP polyclonal antibodies (Santa Cruz Biotechnology), 1:1,000 anti-HA monoclonal antibody (clone 16B12; Covance), 1:1,000 anti-myc monoclonal antibody (clone 9E10; Covance), 1:250 goat anti-DDB1 antibodies (Everest Biotech, Fig. 5c) or 1:500 anti-DDB1 monoclonal antibody (Zymed Laboratories, Fig. S3), and 1:2,000 anti-a-tubulin monoclonal antibody (Sigma-Aldrich). Horseradish peroxidase-conjugated donkey anti-goat IgG (Santa Cruz Biotechnology, 1:5,000), sheep anti-rabbit or anti-mouse IgG (Amersham Biosciences, 1:5,000) were used as secondary antibodies and detection was carried out with ECL (Pierce).

Colony-forming Assay

Singly or doubly transfected HeLa cells were re-plated at lower density 1 day after transfection and cultured in appropriate selection media containing 6 μg/ml blasticidin S (Invitrogen) and/or 200 μg/ml hygromycin B (Chemie Brunschwig). When needed, cells were re-plated after appropriate dilution to avoid cell death due to confluency. Drug- resistant cells were stained with crystal violet (Sigma) on the day indicated in the Figure legends. Note that in Figure 2c, control cells and cells complemented with DDB1(WT^{SiR}) were re-plated six times, whereas DDB1(dm^{SiR}) complemented cells were re-plated three times before staining.

HBV Replication Assay

Viral genome replication was assessed by determining the amount of cytoplasmic core particle-associated HBV DNA three days after transfection as previously described[31], except that quantitation was performed by real-time PCR[45]. Each value is the mean of four separate PCR reactions performed with two primer pairs designed to amplify distinct regions within the HBV genome, one in the polymerase gene and the other within Enhancer I, and two dilutions of the template DNA. Shown are the mean values normalized to transfection efficiency.

Yeast Plasmids and Two-Hybrid Assay

All the proteins are encoded by single-copy plasmids marked with the *TRP1*, *URA3* or *ADE2* gene. VP16-DDB1, VP16-RFX, RFX-HBx, and SV5-V fused to RFX or overexpressed in its native form have been described[33,40]. VP16-DDB1(ΔBPB) and VP16-DDB1(A381E/F382D) were constructed by replacing the region encoding wild- type DDB1 in VP16-DDB1. RFX-WHx was generated by PCR amplifying the WHx coding region from a cloned woodchuck hepatitis B virus genome (J02442; kindly provided to us by Olivier Hantz, INSERM, U871, Lyon) and inserting the resulting fragment into RFX-HBx to replace the HBx coding sequence. RFX-Trpc4AP was constructed in a similar way using a Trpc4-Associated Protein isoform (a) (NM_015638) cDNA clone that was isolated in a yeast two-hybrid screen for DDB1 interactors (O. Leupin and M.S., unpublished). A fragment starting 24 nucleotides upstream of the AUG initiation codon and encompassing the entire Trpc4AP open reading frame was excised from the original clone and inserted in frame C-terminal to RFX, resulting in RFX- Trpc4AP. The β-galactosidase assays were performed in a yeast strain carrying an integrated RFX-dependent *lacZ* reporter gene as described previously[40].

Supplementary Material

Refer to Web version on PubMed Central for supplementary material.

Acknowledgments

We thank ALS synchrotron beamline staff for assistance with data collection; all members of the Zheng lab for invaluable discussions; Wenqing Xu for help and support in our research; and Oliver Leupin for the siRNA-resistant DDB1 clone. N.Z. is a Pew scholar. This study is supported by the Howard Hughes Medical Institute and by BWF PATH award and NIH grant CA107134 to N.Z. and Swiss National Science Foundation 3100A0-100785 and 3100A0-112496 to M.S.

References

1. Hershko A, Ciechanover A. The ubiquitin system. Annu Rev Biochem 1998;67:425–79. [PubMed: 9759494]
2. Pickart CM. Mechanisms underlying ubiquitination. Annu Rev Biochem 2001;70:503–33. [PubMed: 11395416]
3. Petroski MD, Deshaies RJ. Function and regulation of cullin-RING ubiquitin ligases. Nat Rev Mol Cell Biol 2005;6:9–20. [PubMed: 15688063]
4. Angers S, et al. Molecular architecture and assembly of the DDB1-CUL4A ubiquitin ligase machinery. Nature 2006;443:590–3. [PubMed: 16964240]
5. Jin J, Arias EE, Chen J, Harper JW, Walter JC. A family of diverse Cul4-Ddb1-interacting proteins includes Cdt2, which is required for S phase destruction of the replication factor Cdt1. Mol Cell 2006;23:709–21. [PubMed: 16949367]
6. He YJ, McCall CM, Hu J, Zeng Y, Xiong Y. DDB1 functions as a linker to recruit receptor WD40 proteins to CUL4-ROC1 ubiquitin ligases. Genes Dev 2006;20:2949–54. [PubMed: 17079684]
7. Higa LA, et al. CUL4-DDB1 ubiquitin ligase interacts with multiple WD40-repeat proteins and regulates histone methylation. Nat Cell Biol 2006;8:1277–83. [PubMed: 17041588]

8. Nag A, Bondar T, Shiv S, Raychaudhuri P. The xeroderma pigmentosum group E gene product DDB2 is a specific target of cullin 4A in mammalian cells. Mol Cell Biol 2001;21:6738–47. [PubMed: 11564859]
9. Chen X, Zhang Y, Douglas L, Zhou P. UV-damaged DNA-binding proteins are targets of CUL-4A-mediated ubiquitination and degradation. J Biol Chem 2001;276:48175–82. [PubMed: 11673459]
10. Sugasawa K, et al. UV-induced ubiquitylation of XPC protein mediated by UV-DDB-ubiquitin ligase complex. Cell 2005;121:387–400. [PubMed: 15882621]
11. Groisman R, et al. CSA-dependent degradation of CSB by the ubiquitin-proteasome pathway establishes a link between complementation factors of the Cockayne syndrome. Genes Dev 2006;20:1429–34. [PubMed: 16751180]
12. Kapetanaki MG, et al. The DDB1-CUL4ADDB2 ubiquitin ligase is deficient in xeroderma pigmentosum group E and targets histone H2A at UV-damaged DNA sites. Proc Natl Acad Sci U S A 2006;103:2588–93. [PubMed: 16473935]
13. Wang H, et al. Histone H3 and H4 ubiquitylation by the CUL4-DDB-ROC1 ubiquitin ligase facilitates cellular response to DNA damage. Mol Cell 2006;22:383–94. [PubMed: 16678110]
14. Liu C, et al. Cop9/signalosome subunits and Pcu4 regulate ribonucleotide reductase by both checkpoint-dependent and -independent mechanisms. Genes Dev 2003;17:1130–40. [PubMed: 12695334]
15. Higa LA, Mihaylov IS, Banks DP, Zheng J, Zhang H. Radiation-mediated proteolysis of CDT1 by CUL4-ROC1 and CSN complexes constitutes a new checkpoint. Nat Cell Biol 2003;5:1008–15. [PubMed: 14578910]
16. Hu J, McCall CM, Ohta T, Xiong Y. Targeted ubiquitination of CDT1 by the DDB1-CUL4A-ROC1 ligase in response to DNA damage. Nat Cell Biol 2004;6:1003–9. [PubMed: 15448697]
17. Bondar T, Ponomarev A, Raychaudhuri P. Ddb1 is required for the proteolysis of the Schizosaccharomyces pombe replication inhibitor Spd1 during S phase and after DNA damage. J Biol Chem 2004;279:9937–43. [PubMed: 14701809]
18. Kim Y, Kipreos ET. Cdt1 degradation to prevent DNA re-replication: conserved and non-conserved pathways. Cell Div 2007;2:18. [PubMed: 17565698]
19. Wertz IE, et al. Human De-etiolated-1 regulates c-Jun by assembling a CUL4A ubiquitin ligase. Science 2004;303:1371–4. [PubMed: 14739464]
20. Ghosh P, Wu M, Zhang H, Sun H. mTORC1 signaling requires proteasomal function and the involvement of CUL4-DDB1 ubiquitin E3 ligase. Cell Cycle 2008;7:373–81. [PubMed: 18235224]
21. Hu J, et al. WD40 protein FBW5 promotes ubiquitination of tumor suppressor TSC2 by DDB1-CUL4-ROC1 ligase. Genes Dev 2008;22:866–71. [PubMed: 18381890]
22. Li T, Chen X, Garbutt KC, Zhou P, Zheng N. Structure of DDB1 in complex with a paramyxovirus V protein: viral hijack of a propeller cluster in ubiquitin ligase. Cell 2006;124:105–17. [PubMed: 16413485]
23. Wu G, et al. Structure of a beta-TrCP1-Skp1-beta-catenin complex: destruction motif binding and lysine specificity of the SCF(beta-TrCP1) ubiquitin ligase. Mol Cell 2003;11:1445–56. [PubMed: 12820959]
24. Hao B, Oehlmann S, Sowa ME, Harper JW, Pavletich NP. Structure of a Fbw7-Skp1-cyclin E complex: multisite-phosphorylated substrate recognition by SCF ubiquitin ligases. Mol Cell 2007;26:131–43. [PubMed: 17434132]
25. Didcock L, Young DF, Goodbourn S, Randall RE. The V protein of simian virus 5 inhibits interferon signalling by targeting STAT1 for proteasome-mediated degradation. J Virol 1999;73:9928–33. [PubMed: 10559305]
26. Parisien JP, et al. The V protein of human parainfluenza virus 2 antagonizes type I interferon responses by destabilizing signal transducer and activator of transcription 2. Virology 2001;283:230–9. [PubMed: 11336548]
27. Ulane CM, Horvath CM. Paramyxoviruses SV5 and HPIV2 assemble STAT protein ubiquitin ligase complexes from cellular components. Virology 2002;304:160–6. [PubMed: 12504558]
28. Bouchard MJ, Schneider RJ. The enigmatic X gene of hepatitis B virus. J Virol 2004;78:12725–34. [PubMed: 15542625]

29. Sitterlin D, et al. Interaction of the UV-damaged DNA-binding protein with hepatitis B virus X protein is conserved among mammalian hepadnaviruses and restricted to transactivation-proficient X-insertion mutants. J Virol 1997;71:6194–9. [PubMed: 9223516]
30. Sitterlin D, Bergametti F, Tiollais P, Tennant BC, Transy C. Correct binding of viral X protein to UVDDB-p127 cellular protein is critical for efficient infection by hepatitis B viruses. Oncogene 2000;19:4427–31. [PubMed: 10980618]
31. Leupin O, Bontron S, Schaeffer C, Strubin M. Hepatitis B virus X protein stimulates viral genome replication via a DDB1-dependent pathway distinct from that leading to cell death. J Virol 2005;79:4238–45. [PubMed: 15767425]
32. Bontron S, Lin-Marq N, Strubin M. Hepatitis B virus X protein associated with UV-DDB1 induces cell death in the nucleus and is functionally antagonized by UV-DDB2. J Biol Chem 2002;277:38847–54. [PubMed: 12151405]
33. Lin-Marq N, Bontron S, Leupin O, Strubin M. Hepatitis B virus X protein interferes with cell viability through interaction with the p127-kDa UV-damaged DNA-binding protein. Virology 2001;287:266–74. [PubMed: 11531405]
34. Martin-Lluesma S, et al. Hepatitis B virus X protein affects S phase progression leading to chromosome segregation defects by binding to damaged DNA binding protein 1. Hepatology 2008;48:1467–76. [PubMed: 18781669]
35. Chen HS, et al. The woodchuck hepatitis virus X gene is important for establishment of virus infection in woodchucks. J Virol 1993;67:1218–26. [PubMed: 8437213]
36. Zoulim F, Saputelli J, Seeger C. Woodchuck hepatitis virus X protein is required for viral infection in vivo. J Virol 1994;68:2026–30. [PubMed: 8107266]
37. Bergametti F, Bianchi J, Transy C. Interaction of Hepatitis B Virus X Protein with Damaged DNA-Binding Protein p127: Structural Analysis and Identification of Antagonists. J Biomed Sci 2002;9:706–15. [PubMed: 12432237]
38. Cang Y, et al. Deletion of DDB1 in mouse brain and lens leads to p53-dependent elimination of proliferating cells. Cell 2006;127:929–40. [PubMed: 17129780]
39. Wakasugi M, et al. DDB1 gene disruption causes a severe growth defect and apoptosis in chicken DT40 cells. Biochem Biophys Res Commun 2007;364:771–7. [PubMed: 17976535]
40. Leupin O, Bontron S, Strubin M. Hepatitis B Virus X Protein and Simian Virus 5 V Protein Exhibit Similar UV-DDB1 Binding Properties To Mediate Distinct Activities. J Virol 2003;77:6274–83. [PubMed: 12743284]
41. Andrejeva J, Poole E, Young DF, Goodbourn S, Randall RE. The p127 subunit (DDB1) of the UV-DNA damage repair binding protein is essential for the targeted degradation of STAT1 by the V protein of the paramyxovirus simian virus 5. J Virol 2002;76:11379–86. [PubMed: 12388698]
42. CCP4. The CCP4 Suite: programs for protein crystallography. Acta Crystallogr D Biol Crystallogr 1994;D50:760–763.
43. Jones TA, Zou JY, Cowan SW, Kjeldgaard. Improved methods for building protein models in electron density maps and the location of errors in these models. Acta Crystallogr A 1991;47(Pt 2):110–9. [PubMed: 2025413]
44. Brunger AT, et al. Crystallography & NMR system: A new software suite for macromolecular structure determination. Acta Crystallogr D Biol Crystallogr 1998;54(Pt 5):905–21. [PubMed: 9757107]
45. Jamai A, Imoberdorf RM, Strubin M. Continuous histone H2B and transcription-dependent histone H3 exchange in yeast cells outside of replication. Mol Cell 2007;25:345–55. [PubMed: 17289583]

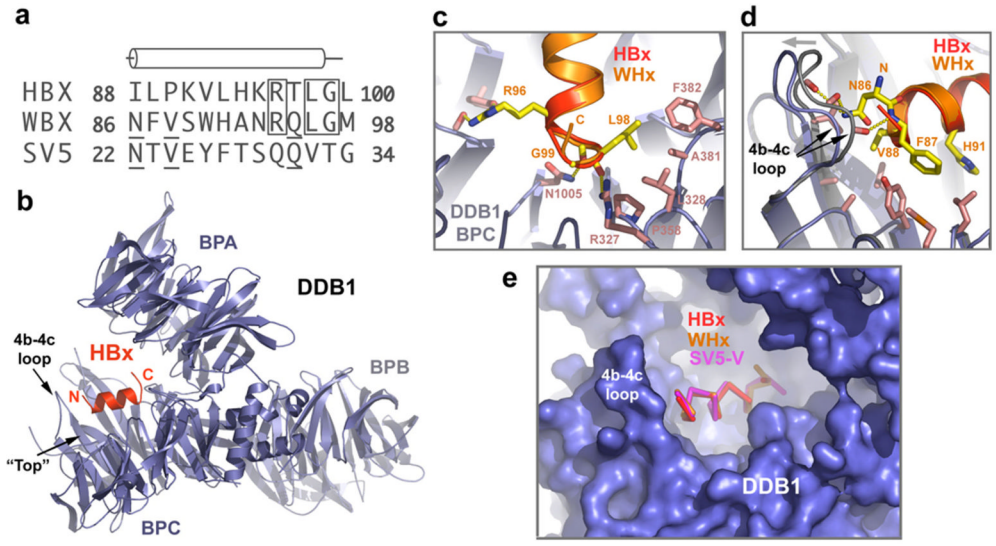

Figure 1.

The hepatitis X proteins bind DDB1 with an α-helical motif. (**a)** Sequence alignment of the DDB1-binding motifs of HBx, WHx, and SV5-V. Strictly conserved residues between HBx and WHx are boxed. Conserved residues between WHx and SV5-V are underlined. (**b)** Overall structure of DDB1 (in blue) in complex with the central helical fragment of HBx (red). The three propeller domains of DDB1 are labeled as BPA, BPB, and BPC. (**c)** The detailed interface between DDB1 and the C-terminal part of the two viral X proteins. HBx (red) and WHx (orange) are superimposed. The three invariant residues (yellow) between HBx and WHx and their surrounding DDB1 residues (pink) are shown in sticks. Yellow dot lines indicate intermolecular hydrogen bonds. (**d)** The detailed interface between DDB1 and the N-terminal part of the two viral X proteins. HBx (red) and WHx (orange) are superimposed. The DDB1-interacting residues of WHx (yellow) and their surrounding DDB1 residues (pink) are shown in sticks. HBx residues are omitted for clarity. The HBx-bound DDB1 BPC domain (blue) and the WHx-bound DDB1 BPC domain (gray) are superimposed to show the conformational differences of the 4b–4c loop in the two crystal structures (also indicated by an arrow). (**e)** Superposition of the DDB1-interacting helical motifs of HBx (red), WHx (orange), and SV5-V (magenta). The DDB1 molecule is shown in surface representation, which outlines the DDB1 BPA-BPC double propeller pocket.

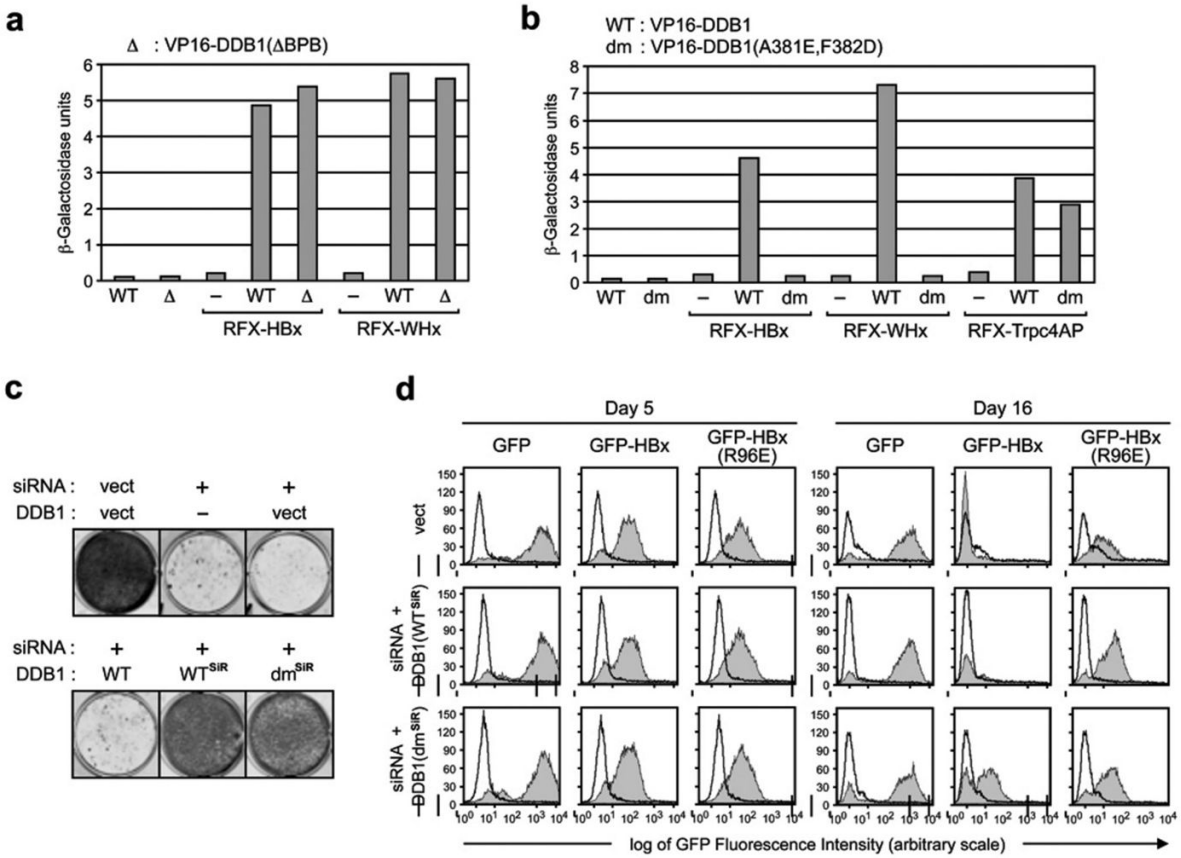

Figure 2.

Binding of HBx helical motif to the DDB1 double propeller pocket is critical for HBx-DDB1 interaction and HBx cytotoxic activity. (**a)** Yeast two-hybrid interaction assay. Wild-type DDB1 (WT) fused to the VP16 activation domain or a truncation mutant lacking BPB (Δ) were tested for interaction with HBx and WHx linked to the transcriptionally inactive human DNA-binding protein RFX. The grey bars represent the relative activities of an integrated *lacZ* reporter gene bearing an upstream RFX-binding site in yeast strains expressing the indicated RFX and VP16 fusion proteins alone or in pairwise combinations. (**b)** The effect of mutating A381 and F382, which are facing HBx-L98 deep inside the DDB1 pocket in the crystal structure, on the binding of DDB1 to HBx, WHx, and, as a control, cellular Trpc4AP was examined in yeast as in **(a)**. dm: DDB1(A381E/F382D) double-mutant. (**c)** Clonogenic cell survival assay. HeLa cells were co-transfected with equal amounts of an episomal vector directing the synthesis of an siRNA against DDB1 (+) together with wild-type DDB1 (WT) or the indicated siRNA-resistant (SiR) DDB1 versions bearing silent mutations in the siRNA-target region. Where indicated, cells were transfected with the respective empty EBB-SUP and EBS-PL parental vectors (vect) or with no vector (−). The transfected cells were cultured for 3 weeks in medium containing blasticidin to select for the siRNA-expression plasmid, and another week in medium containing blasticidin and hygromycin for selection of both plasmids. Drug-resistant cells were fixed and stained with crystal violet 30 days after transfection. Note that cells complemented with the DDB1(A381E/F382D) double mutant proliferate at slightly reduced rates (see Methods). (**d)** HBx lacks cytotoxic activity in cells expressing DDB1 (A381E/F382D) in place of endogenous DDB1. HeLa cells were co-transfected with equal amounts of the DDB1-specific siRNA construct (DDB1-siRNA) together with the siRNA resistant version of either wild-type DDB1 (WT^{SiR}) or the DDB1(A381E/F382D) double

mutant (dm^{SiR}) that cannot interact with HBx, or as a control with the two corresponding empty episomal vectors EBB-SUP and EBS-PL (vect). A GFP gene was co-transfected to assess comparable transfection efficiencies by FACS analysis (data not shown). The transfected cells were cultured in selective medium for 2 weeks as in © before being transduced at high efficiency with lentiviral vectors encoding GFP, GFP-HBx or the DDB1-binding defective GFP-HBx(R96E) point mutant, and further grown under the same selective conditions. The proportion of GFP-positive cells at 5 days and 16 days after transduction was followed by FACS analysis. GFP fluorescence is plotted on a logarithmic scale on the x axis, and cell number is plotted on the y axis. The white FACS profile represents the corresponding untransduced, GFP-negative cells.

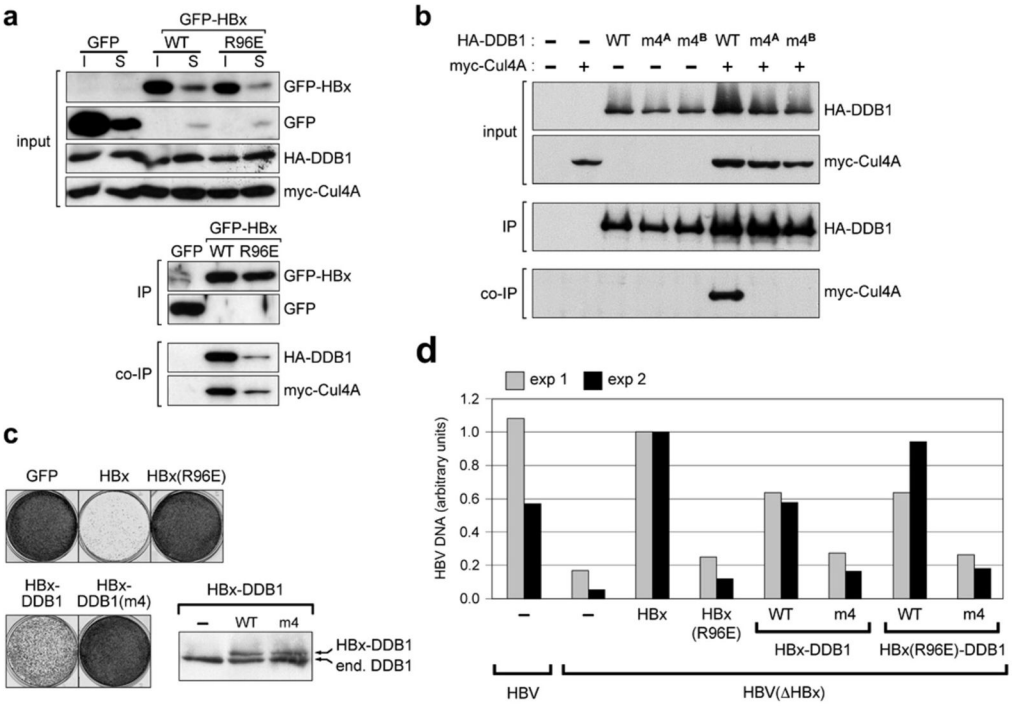

Figure 3.

HBx activities require normal interactions between DDB1 and CUL4. (**a)** HBx forms a ternary complex with DDB1 and Cul4A. HeLa cells were transfected with GFP or the indicated GFP-HBx variants together with HA-DDB1 and myc-Cul4A. Whole-cell extracts were prepared 1 day after transfection and subjected to immunoprecipitation with a monoclonal antibody directed against the GFP epitope. The immunoprecipitates were separated by SDS-PAGE and analyzed by Western blotting for GFP and GFP-HBx using anti-GFP antibodies (IP). The presence of co-immunoprecipitated HA-DDB1 and myc-Cul4A was detected with anti-HA and anti-myc antibodies (co-IP). The upper panels (input) show 1/10 of the input extracts (I) and supernatant fractions (S) from the immunoprecipitations. (**b)** Characterization of a DDB1 mutant defective for Cul4A binding. HeLa cells were transfected with no vector (−) or, either alone or in combination with myc-Cul4A (+) expressed from pcDNA3, wild-type HA-tagged DDB1 (WT) produced from pSrαs, or a DDB1 mutant (m4) with four residues predicted from the crystal structure to be critically involved in Cul4A binding substituted[4]. Whole-cell extracts were prepared 1 day after transfection and subjected to immunoprecipitation with a monoclonal antibody directed against the HA epitope. The presence of immunoprecipitated GFP and GFP-HBx (IP) and co-immunoprecipitated HA-DDB1 and myc-Cul4A (co-IP) was assessed by immunoblotting using antibodies directed against the respective epitopes. The upper panels (input) show 1/10 of the cell extracts used in the immunoprecipitations. HA-DDB1 $m4^A$ and $m4^B$ are transfections of two independent constructs. The data are representative of two separate transfection experiments. (**c)** Clonogenic survival assay of HeLa cells transfected with the indicated control proteins expressed from EBS-PL, which carries a hygromycin resistance marker, or with HBx fused N-terminal to wild-type DDB1 or to the Cul4A-binding defective DDB1 mutant (m4). Previous work has shown that a covalent link between HBx and DDB1 acts as a clamp forcing interaction between the two protein moieties, thereby preventing interaction of HBx with endogenous DDB1[40]. When not made as a fusion protein, a GFP gene was cotransfected to assess transfection efficiencies by FACS analysis. Hygromycin-resistant colonies were fixed and stained with crystal violet 13 days after transfection. On the lower right is a Western blot analysis of the fusion proteins performed with whole-HeLa cell extracts

prepared 3 days after transfection and antibodies to DDB1. The signal corresponding to endogenous DDB1 (end. DDB1) serves as a control for loading. (**d)** HBV replication assay. Human hepatoma HepG2 cells were transfected with a wild-type HBV genomic construct (HBV) or with a variant lacking a functional HBx gene (HBV(ΔX)), and equal amounts of the indicated HBx expression plasmids or the corresponding empty vector (−). A GFP gene was cotransfected to assess comparable transfection efficiencies by FACS analysis (data not shown). Three days after transfection, cytoplasmic HBV core particles were isolated from equal numbers of cells, and the amount of associated HBV DNA replicative intermediates was assessed by quantitative real-time PCR. Results are expressed relative to the replication level of HBV(ΔX) in cells co-transfected with HBx, which was given a value of 1.0. Each value is the mean of four separate PCR reactions performed with two primer pairs designed to amplify distinct regions within the HBV genome and two dilutions of the template DNA. Shown are the results of two independent transfection experiments.

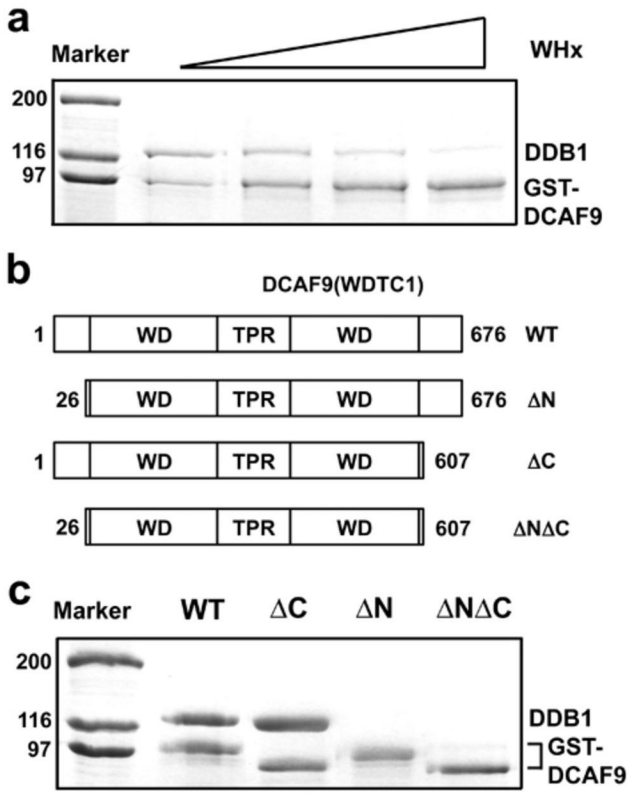

Figure 4.

DCAF9-DDB1 interaction requires a short N-terminal sequence of DCAF9 and can be competed off by the WHx helical motif. (**a)** SDS-PAGE analysis of DCAF9-DDB1 interaction with an increasing amount of WHx peptide. GST-DCAF9 and copurified DDB1 are visualized by Coomassie staining. (**b)** Domain structure of DCAF9 and its truncation mutants used for DDB1 binding analysis. (**c)** Affinity pull-down studies of the interactions between DDB1 and DCAF9 truncation mutants. Copurified DDB1 and DCAF9 mutants are analyzed by SDS-PAGE and visualized by Coomassie staining.

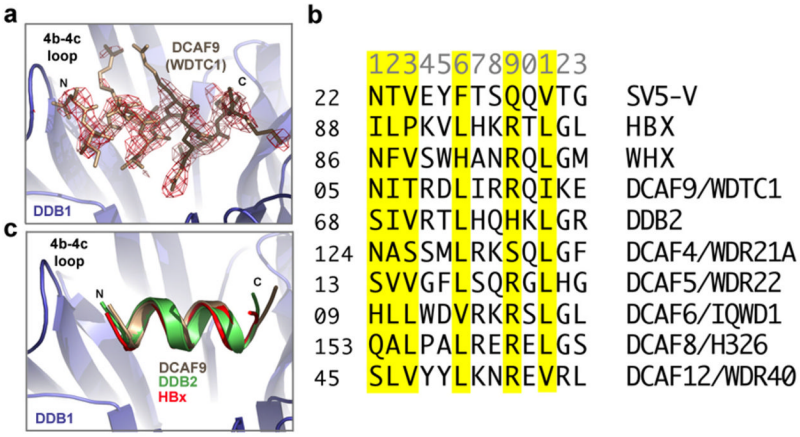

Figure 5.

Identification of the H-box motif in DCAF9, DDB2, and other DCAF proteins. (**a)** A close-up view of the N-terminal helical motif of DCAF9/WDTC1 in complex with DDB1. The DDB1 BPC domain is shown in blue ribbon. The DCAF9 peptide is shown in sticks and colored in wheat, together with its positive *Fo–Fc* electron density calculated and contoured at 3σ before it was built into the complex model. (**b)** Sequence alignment of the H-box motif in the viral and cellular substrate receptors of the DDB1-CUL4 E3 complex. Key DDB1-contacting residues of the H-box motif revealed by the available crystal structures are highlighted by yellow boxes. (**c)** Superposition of the H-box peptides of HBx (red), DCAF9 (wheat), and DDB2 (green) bound to DDB1. The DDB1 BPC domain (in complex with HBx) is shown in blue ribbon. Only the DDB1 molecules from the three complex structures were used for the superposition analysis.

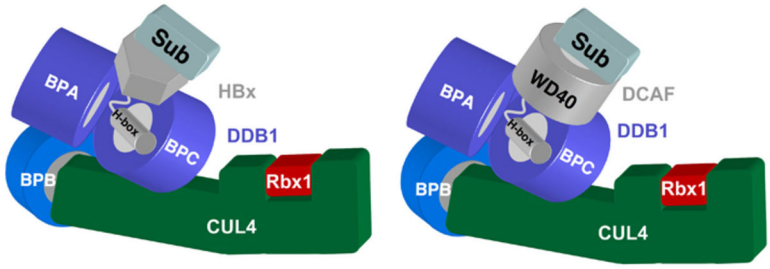

Figure 6.

A schematic model of the assembly of HBx and DCAFs to the CUL4-DDB1 E3 machinery. As a three-propeller protein, DDB1 uses its BPB domain to interact with the N-terminal tip of the CUL4 scaffold, which recruits the RING subunit Rbx1 at the other end. HBx and a typical DCAF protein bind to the DDB1 BPA-BPC double propeller via two interfaces. The H-box motif of HBx and the DCAF protein docks to the “top” surface of the DDB1 BPC domain, while a second domain of HBx and the WD40 domain of the DCAF protein anchor to the DDB1 double propeller, presenting the substrate toward the RING subunit Rbx1, which brings a ubiquitin-charged E2 to the E3 complex.

Table 1

Crystallographic Data Statistics

Data Statistics	DDB1-HBX	DDB1-WHX	DDB1-WDTC1	DDB1-DDB2
Wavelength (Å)	1.000	1.000	1.000	1.000
Resolution (Å)	50–2.9	50–2.8	50–2.8	50–2.8
Space group	P212121	P212121	P212121	P212121
Unit cell (Å) a, b, c	63.9,132.9,183.9	64.1,132.2,184.0	63.6,133.9,183.2	63.7,134.0,182.7
Observations	148453	155095	286244	191003
Unique reflections	32999	38728	39494	39401
Overall I/σ	24.2(3.8)	23.4(2.6)	28.5(2.7)	24.3(2.6)
Completeness (%)	96.9(97.9)	97.8(97.9)	99.9(99.9)	99.0(99.8)
Data redundancy	4.5	4.0	7.2	4.8
R_{merge}[a] (%)	10.1(37.8)	7.0(42.6)	6.7(56.5)	9.1(58.9)
R_{work}[b]/R_{free}	21.6/28.4	21.4/26.7	23.6/29.4	23.0/29.2
Protein atoms (non-H)	8837	8843	8842	8840
Bond rmsd length (Å)/angles(°)	0.049/4.05	0.044/3.70	0.052/4.31	0.046/3.82
Ramchandran plot[c]				
favored (%)	93.5	94.4	92.6	94.0
Disallowed (%)	0	0	0	0

Numbers in parentheses indicate statistics for the highest-resolution data bin.

[a] R_{merge} = • hkl • i|I(hkl)i - < I(hkl) > |/• hkl• i < I(hkl)i >.

[b] R_{work} = • hkl |Fo(hkl) - Fc(hkl)|/• hkl |Fo(hkl)|, where Fo and Fc are observed and calculated structure factors, respectively.

[c] Calculated using the program PROCHECK.